

# Paper 1

Textural and burial effects on rock physics characterization of chalks

By

**Saberi, M.R.**, Johansen, T.A. and Talbot, M.R.

Petroleum Geoscience, 2009

15 (4), 355-365



# Textural and burial effects on rock physics characterization of chalks

Mohammad Reza Saberi\*, Tor Arne Johansen and Michael R. Talbot

*Department of Earth Science, University of Bergen, N-5007 Bergen, Norway*

*\*Corresponding author (e-mail: Mohammad.saberi@geo.uib.no)*

**ABSTRACT:** Velocity behaviour in chalks is determined by a combination of their depositional conditions and subsequent diagenesis. Based on rock physics data from three drill sites on the Ontong Java Plateau, a strategy for velocity modelling is proposed where geological information is imposed via pore structure models.

The Reuss and time-average relations define upper and lower bounds of the velocity data and the self-consistent approximation was applied to find direct links between velocity and changes in microstructure. The latter approach provides an estimate of the dynamic changes of the pore structure as a result of diagenesis in chalks. Depositional pore-models of chalks were determined from environmental conditions and can be defined from textural information. Mechanical compaction and cementation decrease porosity as a function of depth, but may increase the velocity by different rates as the pore structure changes differently. Discrimination between sediment stiffness and pore structure stiffness enables us to justify low velocity for indurated sediments and high velocity for soft sediments. Our results indicate the relevance of the pore structure to velocity interpretation because some variations in velocity data may result from pore structure differences rather than changes in fluid or porosity.

**KEYWORDS:** *carbonate, modelling, reservoir characterization, rock physics, ultrasonic velocities*

## INTRODUCTION

Chalks are pelagic carbonate sediments that are deposited in deep-water environments. Their deposition, as with other carbonates, is very sensitive to changes in oceanographic conditions (e.g. Hamilton *et al.* 1982). Such changes result in variations in their petrophysical and elastic properties (Fabricius 2007). These properties are primarily controlled by the overall porosity reduction resulting from post-deposition (Scholle 1977). Wang (1997) discussed the effects of pore type on the elastic behaviour of carbonates. Eberli *et al.* (2003) demonstrated the relationship between pore type and velocity variations in carbonate rocks. This study shows how geological knowledge can be used to improve modelling of chalk velocity by embedding their predominant pore type within the pore aspect ratio.

The pore aspect ratio (pores are considered as an ideal ellipsoid and the length of the short axis to the length of the long axis defines the pore aspect ratio for each pore) is often used to characterize the pore-space geometry in rocks, and its application ranges from hydrocarbon reservoir characterization to environmental issues. So-called inclusion-based rock physics theories, which seem to be adequate in velocity modelling of carbonates (Agersborg *et al.* 2009), show strong dependence on pore aspect ratios. However, non-uniqueness occurs because a single velocity can be related to different pore-models. Anselmetti *et al.* (1998) introduced a quantitative method for pore-space analysis based on thin-section analysis to quantify and characterize carbonate micro-porosity. On the other hand, Agersborg *et al.* (2009) reported different velocity behaviour for

pores with micro- or meso-scale connectivity. This study indicates some limitations of using thin-section and aspect ratio analysis from scanning electron microscopy (SEM) images for velocity modelling. It means a comprehensive quantification of the effective pore space (pore-space topology) on velocity is very difficult to achieve. Therefore, we usually have to define simpler descriptions that adopt the main geometrical properties of the pore space. However, inversion of seismic velocities or well-log data for a pore aspect ratio model has been studied by many authors, among these Cheng & Toksöz (1979), Sun & Goldberg (1997) and Yan *et al.* (2002). These methods are purely mathematical. Estimated aspect ratios are difficult to link to geological and reservoir characteristics. Furthermore, aspect ratios cannot be measured directly from field data or laboratory measurements, so fixed values of aspect ratios are often used in velocity prediction. However, as has been shown by Yan *et al.* (2002), elastic moduli have nonlinear behaviour with changes in pore aspect ratio. This indicates the limitation of using fixed pore aspect ratios for small depth intervals over which lithology may be regarded as uniform.

In order to overcome these weaknesses and to develop a more accurate model for velocity modelling, we used depositional textures of chalks and diagenesis to constrain our pore-model because these parameters define and modify respectively the initial pore space. Figure 1 shows the possible modifications of the initial pore space as a result of diagenesis for a random packing of hard spheres using a grain consolidation model (Schwartz & Kimminau 1987). This model considers directional grain growth for the solid. Different values of the grain growth exponent ( $k_1$ ) may simulate different

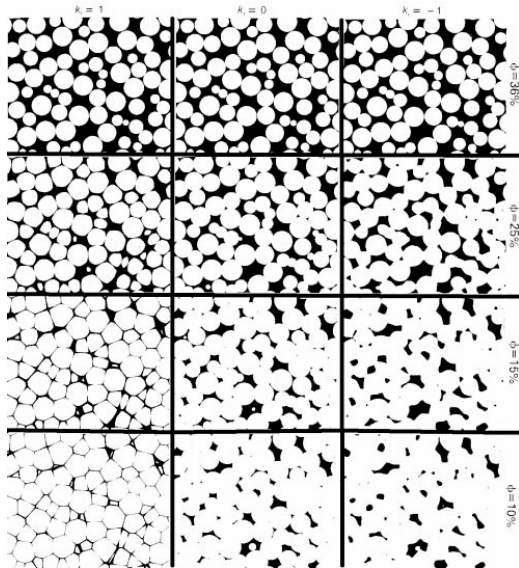


**Fig. 1.** Computer-synthesized cross-section of samples produced by the consolidation of a dense random packing of hard spheres for different porosities. The pore space is shown in black.  $k_1$  is the grain growth exponent, different value of which may simulate different diagenetic processes. For a given porosity, the grain contacts are largest for  $k_1 = -1$  and smallest for  $k_1 = 1$ . For  $k_1 = 0$ , the grains grow equally in all directions (recrystallization);  $k_1 = 1$ , grains grow toward the edge (mechanical compaction); and  $k_1 = -1$ , grains tend to close off the throats (cementation). Compiled from Schwartz & Kimminau (1987).

diagenetic processes. They can be seen as the trend for pore-space changes in different diagenetic realms.

We propose here to use geological information together with expected transformations of the pore-models (Fig. 1) to assist the modelling of chalks. Our strategy has two advantages: (1) it combines geological information and rock physics by establishing a direct link between microstructure and velocity variations; (2) it considers the effects of diagenesis on the pore-model. This opens up the possibility of tracing the diagenetic signature of the sediment from an interpretation of the velocity behaviour versus depth.

We first give a brief review of the main depositional conditions and diagenetic models for chalks. This is followed by the details of our approach. Finally, we demonstrate applications of our model to field data acquired from the Deep Sea Drilling Program (DSDP) and Ocean Drilling Program (ODP) on the Ontong Java Plateau.

### FROM OOZE TO CHALK TO LIMESTONE

Chalks are deep-water pelagic sediments consisting largely of stable low-magnesium calcite. Sedimentation of these pelagic carbonates is relatively simple, involving only deposition from suspension and vertical aggradation followed by burrowing, sediment leaching or lithification to form hard grounds. Most of our knowledge of the initial composition and texture of chalks comes from modern pelagic sediments, which are dominated by planktonic algae (coccolithophores), and zooplankton (e.g. pteropods, heteropods and foraminifera). These mixtures consist of skeletal components of 0.25–1  $\mu$ m-size

coccoliths and 50–100  $\mu$ m-size foraminifera (Morse & Mackenzie 1990) that are modified by environmental factors within the water column and on the seafloor to form soft, water-rich sediments referred to as pelagic ooze. Texture and composition of these pelagic oozes may differ from place to place due to variation in temperature, water chemistry and salinity, latitude, nutrients and carbonate compensation depth. (Hamilton *et al.* 1982; Scholle *et al.* 1983). Røgen *et al.* (2001) used the classification of Dunham (1962) to define the grain-size distribution in chalks where foraminifera (>20  $\mu$ m) are grains and coccoliths (<20  $\mu$ m) form the matrix part. This defines the main depositional texture in chalks, which governs its initial and final porosity. Furthermore, we hereafter use these definitions: (a) mudstones are coccolith-supported and have less than 10% foraminifera content; (b) wackestones are coccolith-supported and have more than 10% foraminifera content; (c) packstones are foraminifera-supported and have more than 10% of coccoliths; and (d) grainstones are foraminifera-supported and have less than 10% of coccoliths. These characteristics of pelagic carbonates are applicable only to upper Jurassic to Holocene chalks (Scholle *et al.* 1983).

The terms ooze, chalk and limestone, which will be used subsequently, simply give three different names to the same deposit as it passes through a continuous spectrum of diagenetic stages. Thus, they discriminate between soft, firm and indurated sediments (Fig. 2). In the ooze interval, mechanical compaction is the main process in reducing porosity (Borre & Fabricius 1998). Mechanical compaction includes dewatering, re-orientation and breakage of grains and reduces ooze porosity along with increasing the induration. In this interval, mechanical compaction forms a more rigid rock frame (Grutzner & Mienert 1999) and dissolution helps to break foraminiferal walls, resulting in smaller fossil fragments (Schlanger & Douglas 1974) or disseminating coccolithophores. Once the carbonate sediment has been mechanically compacted, and a stable grain framework has been established, continued burial will decrease porosity further by recrystallization, chemical compaction (pressure solution) or cementation in a depth interval called a chalk interval (Audet 1995; Grutzner & Mienert 1999; Fabricius 2003; Fabricius & Borre 2007). Recrystallization involves simultaneous dissolution and re-precipitation processes (internal redistribution of calcite), so that some fossil fragments will become larger, smoother and shaped more like crystals. Such a process does not cause porosity loss, but causes the calcite crystals to be more equant and smooth and, in this way, furthers mechanical compaction (Fabricius 2003; Fabricius & Borre 2007), while chemical compaction may supply cements for cementation and thus porosity loss (Scholle 1977).

Cementation becomes the most important factor in reducing porosity in the deeper intervals (limestone interval), where large amounts of cement (internal or external sources) are introduced into the rock (Borre & Fabricius 1998) and mechanical compaction is minimally involved (Fabricius 2003) (Fig. 2). Two different styles of cementation are reported for chalks (Fabricius 2003): contact cementation normally forms from dissolution of unstable minerals (e.g. aragonite) or from redistribution of carbonate ions on the calcite surface (deep-water basins, such as the Ontong Java Plateau) at shallow burial depth; and occluding cementation in deeply buried chalks (limestone interval). Contact cementation normally forms in the case of slow mechanical compaction, welding grains together and stiffening the frame with minor effect on porosity. In contrast, occluding cementation (pore-filling cementation) mainly affects the amount of porosity and stiffens the whole rock. This progressive diagenesis (ooze–chalk–limestone) changes pore structure together with porosity with increasing

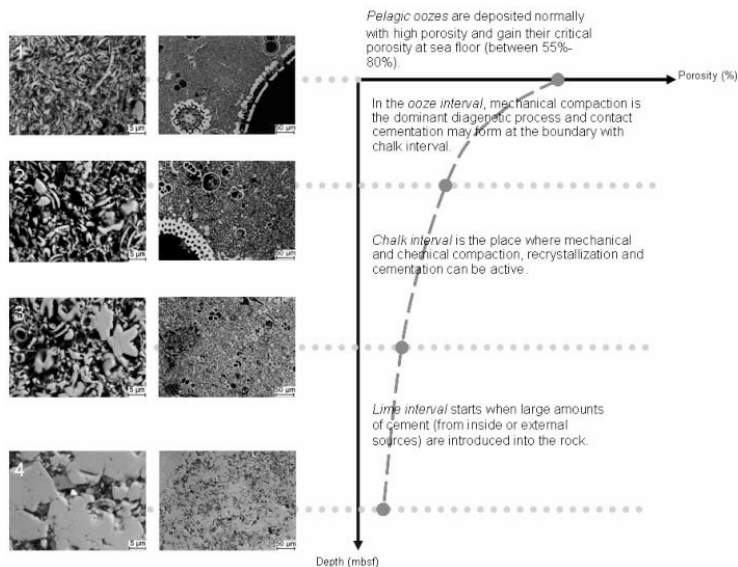


**Fig. 2.** Diagenetic model of chalks. Mechanical compaction reduces porosity and stiffens the frame in the ooze interval. Mechanical and chemical compaction and cementation reduce porosity in the chalk interval. In the limestone interval, cementation is the dominant post-depositional process where calcite crystals are formed in the rock. Images show backscattered electron micrographs from different depths at site 807 (after Borre & Fabricius 1998). (1) depth: 10 m below seafloor (mbsf), porosity: 69%; (2) depth: 319 mbsf, porosity: 57%; (3) depth: 919 mbsf, porosity: 49%; (4) depth: 1127 mbsf, porosity: 17%.

depth, as documented by Kim & Manghni (1992). Processes that generate secondary porosity in pelagic limestones are generally of minor importance (Scholle *et al.* 1983), and we do not consider them in our modelling. Pelagic ooze changes to chalk and limestone by deep burial diagenesis and has already been addressed by many authors (e.g. Schlanger & Douglas 1974; Scholle 1977; Borre & Fabricius 1998; Grutzner & Mienert 1999; Fabricius 2007).

### POROSITY AND PORE-MODELS

Pelagic oozes are typically deposited with high porosity varying between 55% and 85% (Scholle 1977; Hamilton *et al.* 1982; Grutzner & Mienert 1999; Fabricius 2003) depending on sorting and texture. These relatively high values of depositional porosity are related mainly to the content of hollow foraminifera tests (Fabricius 2003) and their granular structure (shapes of coccolithophores and foraminifera). This granular structure is similar to that of sandstones (Nur *et al.* 1998). Positive correlations between foraminiferal content and porosity, mean grain size, velocity and diagenetic potential have been noted previously by others (e.g. Hamilton *et al.* 1982; Audet 1995; Fabricius 2003) and are further confirmed by SEM images that show intragrain porosity within foraminifera tests. However, as has been mentioned by Hamilton *et al.* (1982), the amount of intraparticle porosity depends on the foraminifera's content which may have about 80% of their volume as porosity (Schlanger *et al.* 1973). Combining the Schwartz & Kimminau (1987) grain consolidation model to the above-mentioned observations on chalks (Hamilton *et al.* 1982; Audet 1995; Fabricius 2003), and using Wang's (1997) classification due to Choquette & Pray (1970), chalk porosity effects on velocity (pore-space topology) can be grouped into three main categories of predominant pore types. These groups are denoted as grain porosity, matrix porosity (pore-body, pore-throat and intercrystalline) and crack porosity. Due to the pore-model simplification, one fixed value represents each group aspect ratio. Figure 3a gives a conceptual illustration of these porosities and they are defined in detail in the following text.

*Grain porosity* refers to intragrain porosity (inside foraminifera), which is insensitive to pressure changes and accounts for very stiff pores (represented by  $\alpha=1$ ). Grainstones have a higher amount of grain porosity with stiffer pores than packstone, wackestone and mudstone. Mechanical compaction and dissolution transfers grain porosity to matrix porosity (next group) by breaking foraminifera walls (Hamilton *et al.* 1982).

*Matrix porosity* refers to interparticle porosity, which ranges from compliant to stiff pores (represented by  $\alpha=0.001$  to 0.9) and strongly depends on the overburden pressure. Due to their complex morphology, we simplify these pore spaces to relatively large nodes connected by narrow throats. Matrix porosity can be classified further as matrix porosity/pore-body and matrix porosity/pore-throat. (a) *Matrix porosity/pore-body* is the main and stiffer part of the interparticle porosity. An aspect ratio between 0.1 and 0.9 can be considered representative of this group. (b) *Matrix porosity/pore-throat* (represented by  $\alpha=0.01$ ) considers the connection between two pore bodies in the interparticle porosity. Pore-throats represent compliant parts of the pore-body porosity and can be defined, for instance, at the grain contact area.

In the limestone interval matrix porosity is restricted to the porosity between individual crystals. This porosity, which comprises both pore-body ( $\alpha=0.1-0.9$ ) and pore-throat ( $\alpha=0.01$ ), is considered as matrix porosity/intercrystalline.

*Crack porosity* represents very compliant parts of the porosity, such as cracks and flat pores. They can be defined by very small aspect ratios (in this study they are represented by  $\alpha=0.001$ ) and contribute a small fraction to the total porosity, while having significant influence on velocity (Agersborg *et al.* 2008; 2009). We define these flat compliant pores as very narrow porosities between coccolith crystal elements (before dissemination) or at pore-throats (grain contacts) or even tiny cleavages on foraminifera walls before their breakage (due to the overburden pressure and/or dissolution). These crack-like cavities, as discussed by Agersborg *et al.* (2008), are not important from a geological point of view. However, they can affect the elastic behaviour of the sediment and so are called crack porosity. Figure 3a shows a conceptual figure of this small

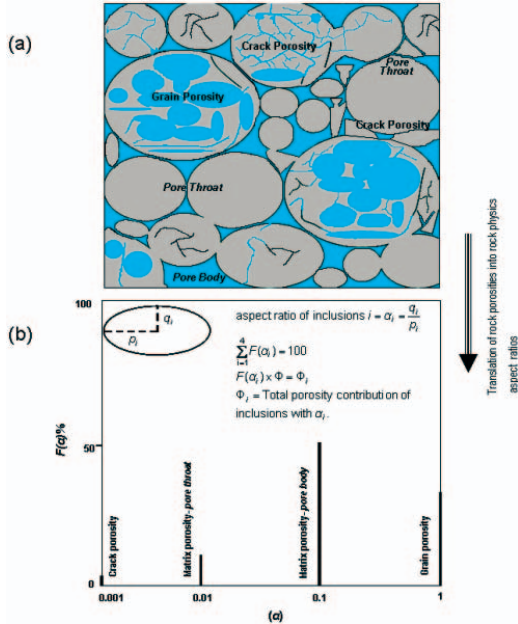


**Fig. 3.** Conceptual illustration of (a) different porosity classes and (b) related pore-model in chalks considered in this study. Grain porosity is the void portion in the foraminifera tests with aspect ratio ( $\alpha$ ) and volume concentration equal to 1 and  $F(1)$ , respectively. Matrix porosity can be subdivided into two parts: pore-body and pore-throat. Pore-body porosity is characterized by aspect ratios of 0.1–0.9 and concentration of  $F(0.1-0.9)$ . This range of aspect ratios stiffens the rock as a function of depth. Pore-throat porosity is defined by an aspect ratio equal to 0.01 with a concentration of  $F(0.01)$ . Crack porosity is the very compliant parts of the porosity, such as cracks and flat pores. These are characterized by aspect ratio 0.001 and concentrations of  $F(0.001)$ . We define these flat compliant pores as very narrow porosities between coccolith crystal elements (before dissemination), at pore-throats (grain contacts) or very small cleavage planes on foraminifera walls before breakage (due to the overburden pressure and/or dissolution).  $\Phi_i$  is the porosity contribution of each pore type in the total porosity. Saturated crack porosity is in blue and unsaturated porosity in black.

fraction of porosity on foraminifera walls before their breakage, which can be created by dissolution (blue lines) and/or overburden pressure (black lines).

In this study, we mimic the chalk pore-space topology (effect of pore space on velocity) based on this porosity classification using a pore-model (the geometrical details of the shapes and spatial distribution of the inclusions). This pore-model (Fig. 3b) takes four aspect ratios of  $\alpha=1, 0.1-0.9, 0.01, 0.001$  for grain, pore-body, pore-throat and crack porosities with volume fractions of  $F_m(1), F_m(0.1-0.9), F_m(0.01)$  and  $F_m(0.001)$ , respectively. Here, 0.1–0.9 indicates the burial stiffening effects on pore-body porosity as the depth increases. Therefore, each modelling point  $m$  can be defined as

$$F_m(\alpha_i) = \{F_m(1), F_m(0.1-0.9), F_m(0.01), F_m(0.001)\},$$

where

$$\sum_{i=1}^4 F_m(\alpha_i) = 100\%, \quad \alpha_i = 1, 0.1-0.9, 0.01, 0.001$$

and  $\Phi_{\alpha_i} = F_m(\alpha_i)\Phi$ .

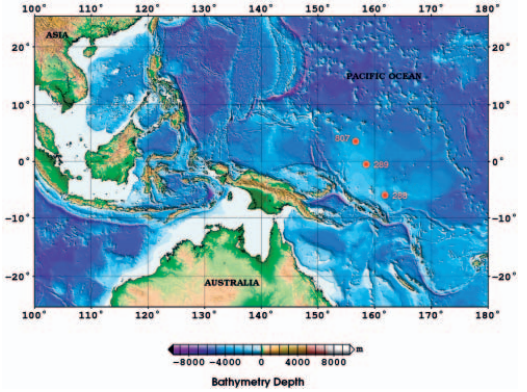


**Fig. 4.** Bathymetric map of the Ontong Java Plateau and three studied sites located there (map generated using Generic Mapping Tool (GMT); bathymetric data from Smith & Sandwell (1997)).

Here,  $\Phi$  is the total porosity, and  $\Phi_{\alpha_i}$  is defined as the volume fraction of the total porosity made up by inclusions of aspect ratio  $\alpha$ . Figure 3 shows a sketch of the porosity classification and the pore-model. It is possible to predict such a model with geological information. Depositional state ( $m=0$ ) can be modelled based on the ooze texture as

$$F_0(\alpha) = \{F_0(1), F_0(0.1), F_0(0.01)\} \quad (2)$$

$F_0(1) = \text{grain contents} \times 0.8$  depending on foraminifera content (Schlanger *et al.* (1973))

$F_0(0.1) = [1 - F_0(1)] \times 0.9$  and

$F_0(0.01) = [1 - F_0(1)] \times 0.1$  depending on the matrix sorting.

In this case, a contribution of 10% pore-throat porosity indicates a small fraction of pore-throats in the matrix porosity as they are defined at the grain contact points. Compaction and cementation from depth point 0 to  $m$  transform  $F_0(\alpha)$  to  $F_m(\alpha)$  by breaking grains, creating crack porosity and making matrix particles growth directionally. The Schwartz & Kimminau (1987) model (Fig. 1) suggests a tendency for mechanical compaction to form sheet-like pores, which implies a softer pore-model in the ooze interval. This tendency is referred to as an increase in specific surface area relative to pore volume with depth by Borre & Fabricius (1998). On the other hand, cementation makes the pore-model stiffer by making more rounded pores and connected particles (Fig. 1). These predicted pore-models are used to constrain the rock physics model and the values of the pore aspect ratio concentrations are determined from the minimum velocity prediction error at each modelling point  $m$ . These determined values may now be given a textural interpretation from velocity data.

## CASE STUDY AND DATA

Ooze, chalk and limestone samples were cored and widely analysed for porosity and P-velocity, among several other parameters, as a part of the DSDP and ODP. This section includes a brief description of the coring, experiments and geological setting of Ontong Java Plateau, followed by a discussion of the rock physics modelling schemes (time-average, Reuss, Voigt and self-consistent approximation).

The studied rock samples are from the Ontong Java Plateau in the western equatorial Pacific (Fig. 4), which is a broad mid-oceanic submarine plateau striking northwest, parallel to

**Table 1.** Rock types occurring at sites 288, 289 and 807

Units	Depth (mbsf)	Description
<b>Leg 30/site 288</b>		
Unit 1	0–466.5	Composed of foram-nannofossil ooze and chalk. Consolidation increases downward from soft ooze to semi-lithified chalk with associated nodular chert. This unit can be divided into two sub-units: 1A (0–82 mbsf) and 2B (82–500(?) mbsf).
—	466.5–533	Unsampled interval – no sample recovery in this interval.
Unit 2	533–988.5	Composed of nannofossil chalk and limestone interbedded with chert, clay and siltstone. This unit can be subdivided into five sub-units: 2A (533–737 mbsf), 2B (737–775 mbsf), 2C (775–814 mbsf), 2D (814–908 mbsf) and 2E (908–988.5 mbsf).
<b>Leg 30/site 289</b>		
Unit 1	0–969	Composed of nanno-foram ooze interbedded with nanno-foram ooze and nanno-foram chalk.
Unit 2	696–1262	Composed of radiolarian-bearing limestone, siliceous limestone, nanno-foram chalk, nanno-foram limestone, nodular chert and tuff. It can be divided into two sub-units based on minerals: sub-unit 2A, consisting mainly of radiolarian-bearing limestone, siliceous limestone, nanno-foram chalk, nanno-foram limestone, and nodular chert; sub-unit 2B, consisting mainly of limestone and tuff.
<b>Leg 130/site 807</b>		
Unit 1	0–968	Composed predominantly of Pleistocene to upper Eocene nannofossil ooze and chalk with foraminifers, with lesser amounts of foraminifer nannofossil ooze and chalk. This unit is divided into sub-units: 1A (0–293 mbsf) and 1B (293–968 mbsf), based on the degree of induration.
Unit 2	968–1351.4	Composed of Eocene to upper Campanian limestone, chert, nannofossil chalk and nannofossil chalk with foraminifers. It is divided into two sub-units: 2A (968–1098 mbsf) and 2B (1098–1351.4 mbsf), based on the transition from chalk to limestone.
Unit 3	1351.4–379.7	Composed of Cenomanian to upper Albian claystone and siltstone with varying amounts of radiolarians, and Albian to Aptian limestone. This unit can be divided into two sub-units: 3A (1351.4–1369.7 mbsf) and 3B (1369.7–1379.7 mbsf), at the transition from claystone to limestone.

Source: Andrews *et al.* (1975), Kroenke *et al.* (1991).

the Solomon Islands to the south (Kroenke *et al.* 1991). The thick cover of pelagic carbonates holds no accumulations of hydrocarbons and was penetrated and studied during Legs 7 (site 64), 30 (sites 288, 289) and 89 (site 586) of DSDP and, more recently, Legs 130 (sites 803–807) and 192 (sites 1183–1187) of the ODP. Our dataset was selected through the DSDP/ODP initial reports and online sources from the different experiments for foraminifer percentage (smear slide analysis), carbonate percentage (carbonate geochemistry analysis), porosity and bulk density (moisture content and mineral densities) and P-velocity measurements on sites 288, 289 and 807.

Onboard the ship, ultrasonic velocities of the sediment cubes, cut from the cores, were measured in both longitudinal (vertical) and transverse (horizontal) directions relative to the core (parallel to the length and across the diameter of the liner) using the pulse transmission technique described by Boyce (1973) (sites 288 and 289) or its modification (site 807). The time of flight of an ultrasonic (400–500 kHz) signal between two transducers of known separation was measured electronically and velocity was calculated. In soft sediments a digital sound velocimeter was employed, while indurated sediments were measured in the Hamilton Frame velocimeter (Boyce 1973). We used only horizontal velocities in our study, because these are less influenced by horizontal fracturing due to the stress released on retrieving the samples, as reported by Fabricius (2003).

These sites were chosen as (1) they have complete datasets (porosity, velocity, carbonate content and smear slide analysis); (2) they penetrated deep enough (especially for site 807) into the sediments to have cores from different diagenetic realms (ooze, chalk and limestone); and (3) ooze, chalk and limestone transitions are more distinct for these sites (especially for site 807). Core recovery results and detailed geological information about the sites are presented in Table 1 and Figure 5.

### EFFECTIVE MEDIUM MODELLING

The relationships between velocity and petrophysical parameters may be obtained using the relevant rock physics

models. Effective-medium models provide estimates of the effective or overall physical properties from knowledge of the mineral and fluid composition and geometrical distributions of the various solid and fluid constituents.

The most often used elastic moduli are the compressional-wave modulus ( $M$ -modulus) and the shear modulus ( $G$ ). These can be expressed from the P- and S-wave velocities ( $V_P$  and  $V_S$ , respectively) and density ( $\rho$ ) by:

$$M = \rho V_P^2, G = \rho V_S^2 \quad (3)$$

With  $\Phi$  denoting the total porosity, the average density is given as

$$\rho = [\rho_{\text{solid}}(1 - \Phi)] + \rho_{\text{fluid}}\Phi \quad (4)$$

where  $\rho_{\text{solid}}$  and  $\rho_{\text{fluid}}$  are the grain and fluid densities, respectively.

The bulk modulus  $K$  is furthermore given as

$$K = [M - (4/3)]G \quad (5)$$

Measurements of the horizontal P velocities range from 1340 m s<sup>-1</sup> to 5840 m s<sup>-1</sup> (typically with 4% error), while the porosity accordingly changes from 74.3% to 4.8%. Porosity and velocity versus depth have the opposite trends, as shown in Figure 5. In order to test predictive models of velocity based on porosity and mineralogy, we test the time-average equation of Wyllie *et al.* (1956) and the boundary models of Reuss (1929) and Voigt (Mavko *et al.* 1998). The time-average equation expresses the effective P-velocity by

$$\frac{1}{V_P} = \frac{(1 - \Phi)}{V_{P,\text{matrix}}} + \frac{\Phi}{V_{P,\text{fluid}}} \quad (6)$$

The Reuss bound defines the elastic moduli from the harmonic average by

$$\frac{1}{K} = \frac{(1 - \Phi)}{K_{\text{matrix}}} + \frac{\Phi}{K_{\text{fluid}}} \quad (7)$$

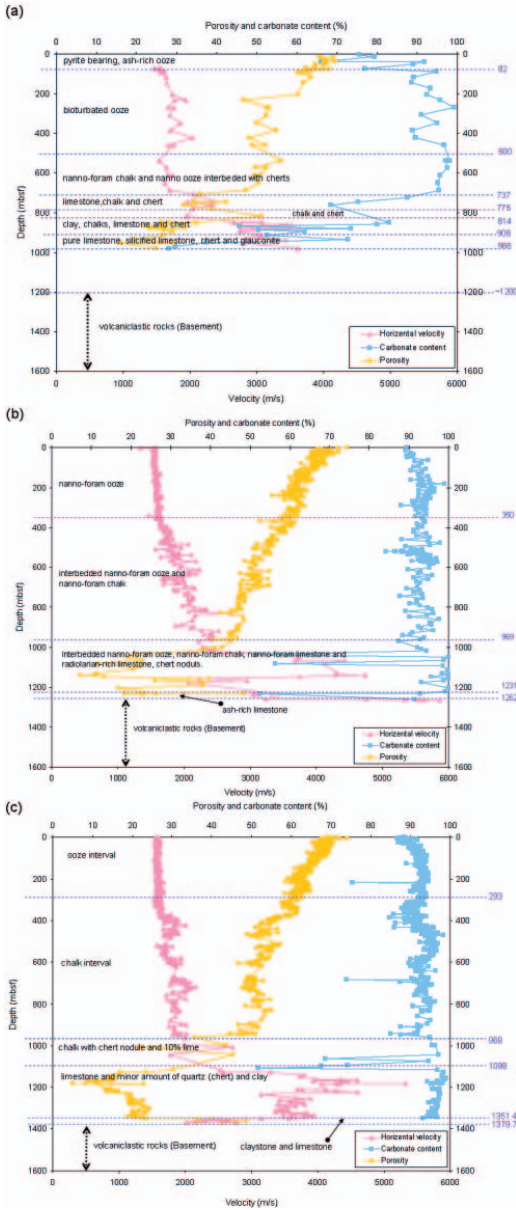


**Fig. 5.** Horizontal velocity, porosity and carbonate content of sites (a) 288, (b) 289 and (c) 807. Interpretation at each site is based on shipboard reports (Andrews *et al.* 1975; Kroenke *et al.* 1991).

where  $\mu=0$ , when  $\mu_{\text{fluid}}=0$  (suspension limit), while the Voigt bound defines the arithmetic mean, i.e.

$$\begin{aligned} K &= [(1 - \Phi)K_{\text{matrix}}] + \Phi K_{\text{fluid}} \\ \mu &= (1 - \Phi)\mu_{\text{matrix}} \end{aligned} \quad (8)$$

Here the subscripts matrix and fluid denote the relevant parameters of the matrix and fluid, respectively.

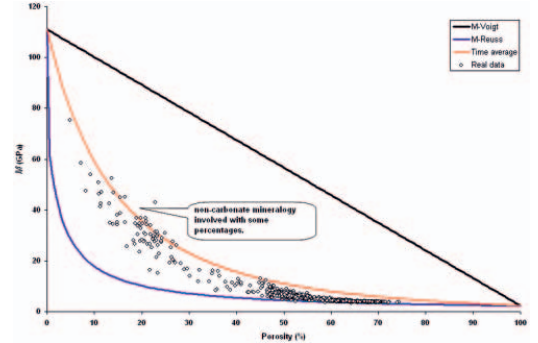


**Fig. 6.** Crossplot of P-wave modulus ( $M$ ) and porosity from ODP carbonate samples (sites 288, 289 and 807), time-average equation (Yyllie *et al.* 1956) and Voigt (Mavko *et al.* 1998) and Reuss (1929) bounds for a composition of calcite and brine. Those points outside the lines (Reuss and time-average) are impure carbonates.

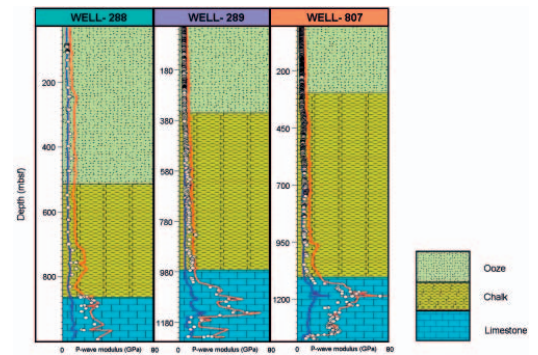


**Fig. 7.** P-wave modulus calculated from Wyllie time-average (red line), Reuss (blue line), and ODP samples (white circles) versus depth for sites 288, 289 and 807. P-wave modulus clearly increases going from ooze to limestone. It starts from the Reuss boundary in the ooze interval and finally reaches the time-average value in limestone. The increase in P-wave modulus with depth indicates the post-depositional stiffening effect. Depths are in metres below seafloor (mbsf).

Comparisons of the measured and predicted values of  $M$  in Figure 6 show that those predicted by Reuss (1929) form a lower envelope of the measurements, while those predicted by the time-average equation form the higher envelope. Figure 7 shows the predicted and measured  $M$  modulus for ooze, chalk and limestone.

Although the Reuss and time-average relations define lower boundary and upper references for the  $M$  values, we still can see some scattering of the data within this interval as  $M$  varies for the same porosity. This effect has been discussed by others (e.g. Anselmetti & Eberli 1993; Agersborg *et al.* 2009) to be related mainly to the pore structure variations due to varying of depositional conditions and post-depositional processes. Eberli *et al.* (2003) stated that pore types in carbonates have nearly the same impacts on the elastic behaviour and sonic velocities as porosity.

First-order scattering models (e.g. Kuster & Toksöz 1974) are restricted to handling a dilute volume fraction of pores (lower porosity rocks) while the self-consistent approximation (SCA) mimics the effects of second- and higher-order scattering terms due to pore-to-pore interactions. SCA is used to

**Table 2.** Elasticity data selected on the basis of citation in Fabricius (2002)

Mineral	$\rho$ (g cm <sup>-3</sup> )	$K$ (GPa)	$M$ (GPa)	$G$ (GPa)	$V_p$ (m s <sup>-1</sup> )	$V_s$ (m s <sup>-1</sup> )
Calcite	2.71	71	111	30	6400	3300
Brine	1.02	2.3	2.3	0	1500	0

$\rho$ , density;  $K$ , bulk modulus;  $M$ , P-wave modulus;  $G$ , shear modulus;  $V_p$ , P-wave velocity;  $V_s$ , S-wave velocity.

study either a fluid containing solid grains or a solid containing fluid-filled pores. It models a more concentrated volume fraction of isolated inclusions than Kuster–Toksöz (1974) by incorporating their elastic interactions in the effective medium formulation. The pore–pore interactions here are elastic and not those due to fluid flow. Berryman (1980*a, b*) formulated SCA for porous rocks where a uniform host material embedded spherical and ellipsoidal inclusions.

Suppose  $N$  families of inclusions each of aspect ratio  $\alpha$  are embedded in a host medium with density, bulk modulus and shear modulus of  $\rho^*$ ,  $K^*$  and  $\mu^*$ . Berryman (1980*b*) derived the general expressions for the self-consistent elastic constants of the composite materials based on assumptions that the net scattering is zero, whenever  $\rho^*$ ,  $K^*$  and  $\mu^*$  represent those of the effective physical properties, i.e.

$$\begin{aligned} \rho^* &= (1 - \Phi)\rho_m + \sum_{i=1}^N \Phi_i \rho_i, \\ \sum_{i=1}^N \Phi_i (K_i - K^*) \times \mathbf{P}^{*i} &= 0, \\ \sum_{i=1}^N \Phi_i (\mu_i - \mu^*) \times \mathbf{Q}^{*i} &= 0. \end{aligned} \quad (9)$$

$\mathbf{P}^{*i}$  and  $\mathbf{Q}^{*i}$  are tensors that depend on the material properties of the matrix and the inclusion material as well as the aspect ratios of the inclusions. Formulae for prolate and oblate spheroids and disc shapes are found in Berryman (1980*a, b*). The SCA method is a high-frequency approximation (Mavko *et al.* 1998) and predicts percolation limits at critical porosity. This means it simulates high-frequency saturated rock behaviour and is therefore appropriate to apply to ultrasonic laboratory conditions. In this study we simulate saturated high-frequency P-wave velocity measurements using SCA and expected pore-models at each modelling point  $m$ . Pore-model determinations are discussed earlier in the porosity and pore-models subsection.

## MODELLING RESULTS

The elastic moduli of the samples were modelled based on prescribed changes in aspect ratios with increasing depth for sites 288 ( $m=6$ ), 289 ( $m=8$ ) and 807 ( $m=12$  and 111). Modelling was performed at seven ( $m=6$ ) and nine ( $m=8$ ) points for sites 288 and 289, respectively. Because site 807 has the longest penetration in deep-basin sediments, as well as a complete dataset, modelling was performed with two different grid densities (13 and 112 points). Thirteen points ( $m=12$ ) was chosen for consistency in comparing the results with sites 288 and 289, while 112 points ( $m=111$ ) is for detailed pore-model interpretation ( $m=0$  denotes depositional condition). The mono-mineralogical chalk is saturated with brine (Table 2), which introduces errors in the modelling when either mineralogy or saturation status is changed. The modelling points, however, were chosen where the carbonate contents are high and show a large variation relative to their neighbours with the

same porosity. This highlights pore-model effects on the velocity variations. Table 3 presents the parameters used in the modelling (seven, nine and thirteen points) at these three sites (288, 289, and 807, respectively). Figure 8 shows a comparison between measured and modelled velocities. The resulting pore-throat concentrations ( $F(0.01)$ ) show a distinct increase in the limestone interval (Table 3). This increase may be related to the appearance of crystals and as a result of intercrystalline porosity instead of pore-body and pore-throat porosities.

From the SCA modelled velocities of sites 288, 289 and 807, it is possible to display nonlinear curves denoting a set of fixed aspect ratios (FAR) at about 800 mbsf (Fig. 9*a, b, c*) that lie within the Ruess and time-average curves. Each FAR curve represents a fixed pore aspect ratio used for the modelling of each point. These curves transform from the depositional to the final due to the effect of post-depositional processes. On the other hand, if porosity reduction of the sediment was not accompanied by the changes in pore-model, then  $M$  would be expected to increase following the depositional FAR curve. In reality, diagenetic alterations change the pore-model curves from one to another and may show totally different behaviour from place to place. The behaviour of FAR curves is related to diagenetic potential and can be considered responsible for scattering in velocity with the same porosity. Figure 9 compares these curves for depositional ( $m=0$ ) and final ( $m=4, 3$  and 7 for sites 288, 289 and 807, respectively) states (limestone interval) at about 800 mbsf. Our approach assumes that any change in the pore-model is forced by diagenesis, which may indicate different changes in the pore-space topology (and hence the effect of pore space on velocity) for site 288 compared to sites 289 and 807. On the other hand, the same depositional FAR curve for the three sites may also indicate the same depositional condition (texture) in the whole area (Fig. 9).

## DISCUSSION

The pore-model  $F_m(\alpha)$  described above can explain velocity variations even with the same porosity. In order to establish a link between  $F_m(\alpha)$  and microstructural changes, we need to characterize the pore-model by properties related to pore-model stiffness, pore-model crystallinity, pore-model stability and diagenetic potential.

The *pore-model stiffness* (PMS) indicates the stiffness of the pore system, and it increases with increasing amount of spheroidal pores (i.e.  $\alpha=1$ ). We define a rms. value representing the PMS at each modelling point by

$$(PMS)_m = \left[ \frac{1}{N} \sum_{i=1}^N (F_m(\alpha_i) \alpha_i)^2 \right]^{1/2} \quad (10)$$

where  $N$  is the number of pore classes in the pore-model ( $\alpha_i = \{1, 0.5, 0.01, 0.001\}$ ).

The *pore-model crystallinity* indicates the contribution of the pore-throat porosity in the total porosity (e.g. value of  $F(0.01)$  in the model). When crystalline calcite cement is introduced into the rock (limestone interval), pore-body and pore-throat porosity definitions will change as porosity is mainly between planar crystal faces. A change toward intercrystalline porosity will affect the pore-model mainly through an increase in  $F(0.01)$ .

The *pore-model stability* shows the contribution of crack porosity in the pore-model. The total crack density ( $\epsilon$ ) can be defined as  $\epsilon = 3F(\alpha)/4\pi\alpha$ , which, for example, gives the crack volume concentration for  $\alpha=0.001$  as  $F(0.001) = 0.0042\epsilon$ . This equation implies low concentration of cracks in the model. The geological information supports this implication.

**Table 3.** Modelling parameters for sites 288 (m=6), 289 (m=8) and 807 (m=12)

m	Depth (m)	$\Phi$ (%)	Aspect ratio concentration- $F(a)$ (%)				$V_{pm}$ (m s <sup>-1</sup> )	$V_{pr}$ (m s <sup>-1</sup> )	Description
			$\alpha=1$	0.1/0.9	0.01	0.001			
<b>Leg 30/site 288</b>									
0	80	65	32	64 (0.1)	4	0	1596	1570	Ooze
1	420	48	0	70 (0.1)	25	5	2000	2040	Ooze
2	580	53	24	66 (0.2)	5	5	1682	1660	Ooze, chalk & chert
3	745	41	0	75 (0.2)	15	10	1960	1970	Chalk, lime & chert
4	800	43	2.5	70 (0.5)	22.5	5	2009	2000	Chalk & chert
5	900	28	3	70 (0.6)	21	6	2756	2800	Clay, chalk, lime & chert
6	980	25	0	69 (0.6)	30	1	3628	3620	Lime, chert
<b>Leg 30/site 289</b>									
0	50	66.5	50	45 (0.1)	5	0	1568	1550	Ooze
1	300	60	45	40 (0.2)	10	5	1636	1630	Ooze
2	500	51	44	50 (0.2)	5	1	1950	1960	Ooze & Chalk
3	800	47	40	54 (0.3)	5	1	2169	2150	Ooze & Chalk
4	1100	22	48	42 (0.5)	7	3	4232	4200	Ooze, Chalk, Lime & Chert
5	1138.3	7.1	0	35 (0.5)	62	3	4753	4740	Limestone interval
6	1147.8	13.2	0	29 (0.5)	68.2	2.8	3752	3750	Limestone interval
7	1215	20.7	2	39 (0.6)	56	3	3233	3230	Limestone interval
8	1234.4	23.1	0	24 (0.8)	76	0	3049	3050	Limestone interval
<b>Leg 130/site 807</b>									
0	0	72	32	56.4 (0.1)	11.6	0	1574	1570	Critical porosity
1	100	65	30	62.6 (0.1)	5.4	2	1576	1570	Mechanical compaction
2	290	63	28	65 (0.1)	6.5	0.5	1653	1660	Contact cementation
3	340	58	20	74 (0.2)	5	1	1689	1690	Compaction
4	440	52	46	52 (0.2)	1	1	1896	1900	Higher fraction of forams
5	550	51	15	80 (0.6)	2	3	1678	1680	Lower fraction of forams
6	730	50	48	47.5 (0.4)	4	0.5	2052	2050	Higher fraction of forams
7	830	50	28	57 (0.4)	12.6	2.4	1848	1850	High pore-throats
8	1006.8	21.7	10	55 (0.5)	20	15	2716	2720	Reduce forams
9	1127.6	16.9	0	30 (0.6)	64.6	5.4	3279	3280	Occluding cements
10	1180	8.2	0	18 (0.2)	82	0	4272	4270	Well-sorted limestone
11	1209.5	13.9	0	21 (0.8)	79	0	3687	3690	Poorly sorted limestone
12	1303	24.2	0	54 (0.6)	46	0	3465	3460	Compact limestone

Based on geological information at each site and general diagenetic model, one preliminary pore-model is considered. These pore-models are modified by measured velocities ( $V_{pr}$ ) and by using a SCA method. Important factors that affect the preliminary pore aspect ratios are explained briefly in the description column. Notice that the pore-throat aspect ratio concentration increases strongly when lithology changes to limestone. This shows crystallinity at  $m=9, 10, 11$  and  $12$  for site 807 while it is at  $m=5, 6, 7$  and  $8$  for site 289.  $V_{pm}$  is the modelled P-velocity and  $\Phi$  is the total porosity.

The *diagenetic potential* ( $\Delta F_m$ ) is a qualitative term introduced by Schlanger & Douglas (1974) and shows the degree of lithification of a carbonate sediment at a given depth. It is possible to express this term as a quantitative value by using the

pore-model because diagenesis changes the initial pore-model. It can be defined as

$$\Delta F_m(a)\% = [F_m(a) - F_0(a)] \times 100, \quad (11)$$

$$a = 1, 0.1 - 0.9, 0.01, 0.001$$

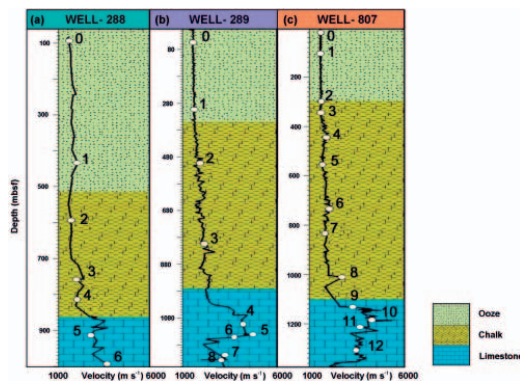
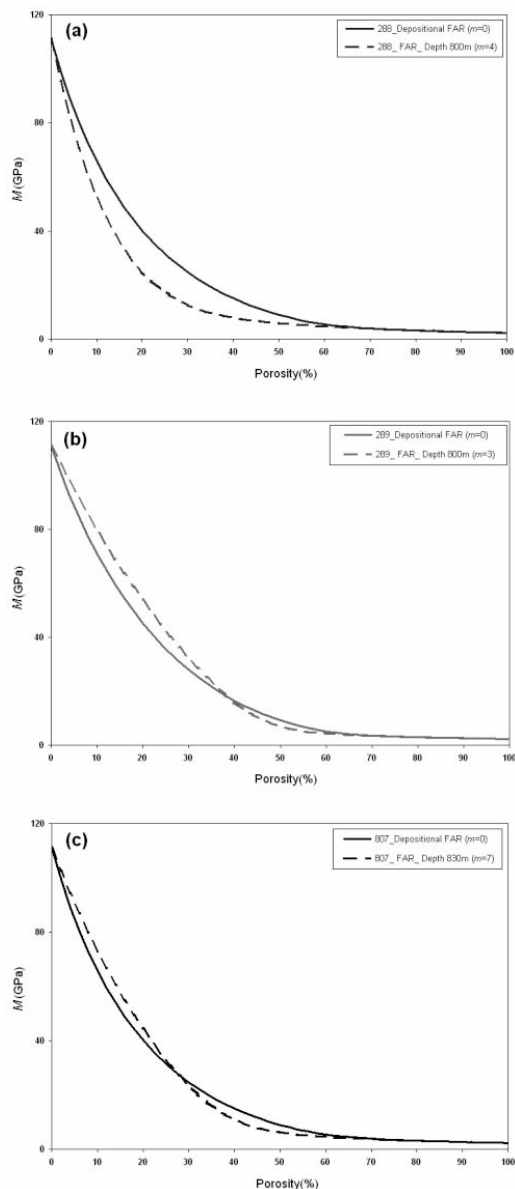


**Fig. 8.** Comparison of SCA modelled velocities (white circles) and measured data (black lines) for (a) site 288, (b) site 289 and (c) site 807. Depths are in metres below seafloor (mbsf).

Figures 10, 11, and 12 present the results of the velocity modelling ( $m=111$ ) at site 807. Figure 10 shows diagenetic potential ( $\Delta F_m(a)$ ) for different porosity classes (grain, matrix and crack porosities). Figure 11 depicts the values of PMS for different intervals (ooze, chalk, limestone). Figure 12 displays the regular stiffening trend of pore bodies (0.1–0.9) and the interpreted anomalies.

PMS decreases from 0.25 in the ooze interval to 0.17 for the chalk interval (Fig. 10). This decrease implies that the pore-model is softened by mechanical compaction although the rock frame is stiffened. PMS increases in the limestone interval (Fig. 11), which implies cementation effects since it is the dominant process in the limestone interval. Based on these observations, important factors affecting the pore topology in chalks can be related to texture, mechanical compaction and cementation.

*Texture* is a category that includes several features of the constituent particles, such as size, sorting, packing, fabric, shape and roundness (Gutierrez *et al.* 2002). An important textural factor in chalks is the grain-size distribution (sorting) and packing. Sorting and packing are both determined by



depositional conditions and affect reservoir quality through porosity and permeability and thereby also affect the reservoir elastic properties (Dvorkin & Gutierrez 2001). As observed by Fabricius *et al.* (2007) on chalk samples from the North Sea, sorting of the mud-matrix controls the porosity to a large extent. It also has a significant effect on the elastic behaviour, because it means a stiffer pore-model from mudstone to grainstone as the  $F(1)$  fraction increases. In general, grainstones should have higher velocities than mudstones and wackestones at a given porosity. Packing (e.g. cubic to rhombohedral) also plays an important role in the diagenetic potential and the reservoir property variations for a given rock type. The blue bars in Figure 12 can be related to the well sorted (fewer contact points, therefore softer framework) carbonate particles. These points also exhibit low-angle truncation surfaces as an indicator of well-sorted sediments (Kroenke *et al.* 1991).

*Mechanical compaction* can be related to changes in aspect ratios due to the changes in differential pressure, as discussed by Nur & Simmons (1969), Sun & Goldberg (1997) and Yan *et al.* (2002). They all discussed the dynamic behaviour of aspect ratios with pressure. The same behaviour can be followed in our modelling results (Fig. 11) by progressive diagenesis versus depth as the pore-model softens constantly (PMS decreases). In the ooze interval, where mechanical compaction is dominant, pore-body porosity changes to pore-throat porosity, while crack porosity can be formed by dissolution or by overburden pressure on foraminifera walls or at grain contacts (Fig. 2). This introduces a small amount of crack porosity into the system at about 100 m. These crack porosities vanish due to closing when passing into the limestone and where large volumes of cement are introduced into the system. In the chalk interval, mechanical compaction reduces PMS by changing grain porosities into pore-body and pore-throat porosities as well as increasing pore-throat and crack porosity contributions. Cementation increases PMS by increasing the contribution of pore-body porosities and making the pores stiffer. This inhomogeneous cementation imposes some scattering in the data, as seen in Figure 11.

*Cementation* in chalks either increases grain contact strength or acts as a pore-filling agent (Fabricius 2003). Figure 12 compares different pore-body aspect ratios within the depth interval. The parts with relatively higher aspect ratios (red bars) may indicate the effect of contact cementation. The increase in the PMS (Fig. 11) for the limestone interval can be linked to pore-filling cementation.

**Fig. 9.** Depositional ( $m=0$ ) and final fixed aspect ratio (FAR) curves for (a) site 288, (b) site 289 and (c) site 807 compared at about 800 mbsf. Depositional FAR curves ( $m=0$ ) simulate P-wave modulus ( $M$ ) versus porosity ( $\Phi$ ) behaviour as if the depositional pore-model was unchanged during diagenesis. Final FAR curves (for  $m=4, 3$  and  $7$  for sites 288, 289 and 807, respectively) simulate  $M$  versus  $\Phi$  behaviour with the pore-model compared at about 800 mbsf. Depositional FAR curves for the three sites are almost the same, which shows similarity between their depositional conditions (textures). Final FAR curves for sites 289 and 807 are similar to depositional curves, whereas for site 288, changes are more significant. This suggests a different evolution from the depositional pore-model in site 288 compared to pore-model evolutions in sites 289 and 807. Because, in our modelling approach, we assumed diagenetic intensity is responsible for pore-model changes, we can conclude that the diagenetic effects on pore-space topology (and hence the effect of pore space on velocity) are different for site 288 in contrast to sites 289 and 807. The pore-model stiffness (PMS), which is defined as the rms. value of the aspect ratio concentrations (equation (10)), also reveals similarity in the pore-model evolutions for sites 289 and 807. Depositional PMS values are almost equal for the three sites (depositional PMS=0.23). However, final PMS changes to about 0.08 for sites 289 and 807, while it takes a higher value for site 288 (final PMS=0.09) (Table 3).

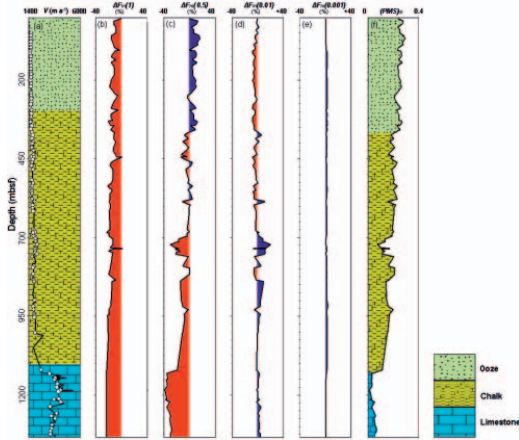


**Fig. 10.** Velocity modelling at site 807 for 112 modelling points ( $m=111$ ). (a) Comparison between modelled and measured velocities; (b) diagenetic potential of grain porosity ( $\Delta F_m(1)$ ) in percent; (c) diagenetic potential of pore-body porosity ( $\Delta F_m(0.5)$ ) in percent; (d) diagenetic potential of pore-throat porosity ( $\Delta F_m(0.01)$ ) in percent; (e) diagenetic potential of crack porosity ( $\Delta F_m(0.001)$ ) in percent; and (f) pore-model stiffness ( $PMS$ ) $_m$  ( $PMS$ ) $_m$  decreases from the ooze interval to the limestone interval. It begins with a PMS value of about 0.25 for ooze, then decreases to a value about 0.17 for the chalk interval and about 0.05 for the limestone interval.

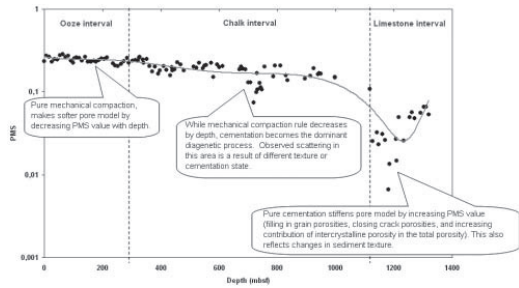


**Fig. 11.** Pore-model stiffness (PMS) versus depth for site 807 ( $m=111$ ). In general, the PMS value decreases with depth for the ooze interval (pure mechanical compaction) and chalk interval (mechanical compaction and cementation). Different cementation or textural states in the chalk and limestone intervals cause scattering. In the limestone, cementation increases stiffness by filling in the grain porosities, closing cracks and increasing the contribution of inter-crystalline porosity relative to the total porosity. This may also indicate changes in the sediment texture (Fabricius & Borre 2007).

Other factors may affect the pore-model, which we did not consider here, such as pore fluid pressure and early hydrocarbon introduction. Both cause a reduction in the diagenetic potential of the sediment and cause the pore aspect ratio transformation to become very slow or absent ( $\Delta F_m(\alpha) \sim 0$ ). As a result, the depositional pore-model will be applicable to the whole sediment column.

Fabricius (2003) suggested a modelling approach named the 'isoframe model' in chalks using the modified upper Hashin-Shtrikman bound (Nur *et al.* 1998). This approach is relatively easy to link to petrographic data; it assumes that all pores are spherical and homogeneously mixed. This means that velocity is modelled in accordance with overall stiffness, while pore structure variations are ignored. Here, we distinguish sedi-

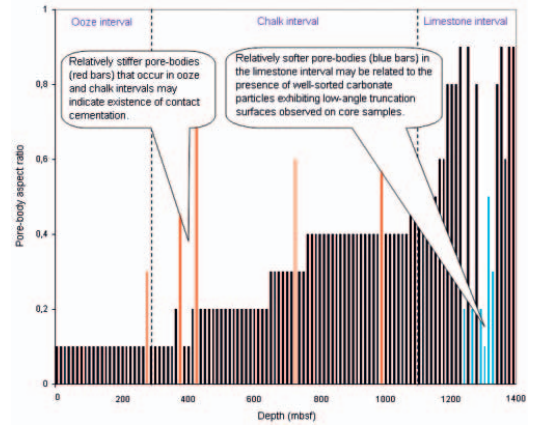


**Fig. 12.** Pore-body aspect ratio variation by depth for site 807 ( $m=111$ ). Depths are in metres below seafloor. A gradual increase in pore-body aspect ratio versus depth is observed. There are some abnormally high aspect ratios in ooze and chalk interval (red bars), which indicates stiffer pore-bodies. This can be a result of contact cementation at those points. Lower aspect ratios in limestone interval (blue bars), as observed on core samples, are related to well-sorted carbonate particles.

ment stiffness from the effect of pore space on velocity (pore-space topology) through the PMS parameter. This will be useful in modelling the zones with the same porosity but different velocities (such as  $m=4, 5$  and  $6$  on site 807). Other uncertainties in determining velocity with this approach can be summarized as follows:

- pore shape in a real rock is not perfectly ellipsoidal as assumed in the SCA approach;
- describing the pore spectrum by just four fixed aspect ratios (1, 0.1–0.9, 0.01 and 0.001), each representing a porosity class (grain, pore-body, pore-throat and crack porosities, respectively), is a simplification;
- different authors report different percentages for foraminiferal hollow parts (Hamilton *et al.* 1982). Because we did not have access to the SEM images and their petrographic analyses of the wells in our area of study, the analysis of Schlanger *et al.* (1973) from site 167 near this area was used. Based on a petrographic and textural approach utilizing SEM photos of pelagic sediments at site 167, they suggest 80% porosity for foraminifera tests. Specifying foraminifera types and porosities for different depths at each site can help to improve the results.

Our modelling results indicate that these uncertainties do not have a major impact on velocity modelling for this area.

## CONCLUSIONS

This paper incorporates geological information and burial effects on rock physics modelling of chalks. The concepts of a porosity classification in chalks based on foraminifera content and pore aspect ratio transformation according to diagenetic alteration are key to implementing burial effects into the modelling. The modelling reveals the effect of depositional texture and post-depositional processes on velocity variations in a mono-mineralogical chalk. It should, therefore, be possible to discriminate between different depositional textures and post-depositional processes from velocity data. This direct link

between microstructural changes and pore aspect ratio transformation may help to improve prediction of velocity variations due to changes in texture and diagenesis. It can also help with detailed seismic reservoir characterization using a velocity model from seismic data when adapted to the low-frequency behaviour of a seismic velocity model.

Our study also reveals how different porosity-reducing diagenetic processes, such as mechanical compaction and cementation, may change the velocity by different rates as one process can soften, and another stiffen, pore-models, respectively. We introduced various terms to characterize the pore-model. In particular, the pore-model stiffness indicates the elastic behaviour of pore structure (pore-space topology) and the pore-model crystallinity is an indicator of intercrystalline porosity. The diagenetic potential term points to the degree of diagenetic alteration and indicates chalk lithification.

This work was made in collaboration with IRIS and funded by the Norwegian Research Council Petromax Program under contract 163316 (Carbonate Reservoir Geomodel). The authors acknowledge Ida Lykke Fabricius for sharing site 807 data. Thanks also to Remy Ågersborg for discussions on the rock physics part and Kyle T. Spikes for comments.

## REFERENCES

- Ågersborg, R., Johansen, T.A., Jakobsen, M., Sothcott, J. & Best, A. 2008. Effects of fluids and dual-pore systems on velocities and attenuations of carbonates. *Geophysics*, **73**(5), N35–N47.
- Ågersborg, R., Johansen, T.A. & Jakobsen, M. 2009. Velocity variations in carbonate rocks due to dual porosity and wave-induced fluid flow. *Geophysical Prospecting*, **57**(1), 81–98.
- Andrews, J.E., Packham, G. & Eade, J.E. *et al.* 1975. *The shipboard scientific party, initial reports of Deep Sea Drilling Project*, **30** (e-book).
- Anselmetti, F.S. & Eberli, G.P. 1993. Controls on sonic velocity in carbonates. *Pure and Applied Geophysics*, **141**, 287–323.
- Anselmetti, F.S., Luthi, S. & Eberli, G.P. 1998. Quantitative characterization of carbonate pore systems by digital image analysis. *American Association of Petroleum Geologists Bulletin*, **82**(10), 1815–1836.
- Audet, D.M. 1995. Modelling of porosity evolution and mechanical compaction of calcareous sediments. *Sedimentology*, **42**, 355–373.
- Berryman, J.G. 1980a. Long-wavelength propagation in composite elastic media I. Spherical inclusions. *Journal of Acoustic Society of America*, **68**(6), 1809–1819.
- Berryman, J.G. 1980b. Long-wavelength propagation in composite elastic media II. Ellipsoidal inclusions. *Journal of Acoustic Society of America*, **68**(6), 1820–1831.
- Borre, M.K. & Fabricius, I.L. 1998. Chemical and mechanical processes during burial diagenesis of chalks: An interpretation based on specific surface data of deep-sea sediments. *Sedimentology*, **45**(4), 755–769.
- Boyce, R.E. 1973. Physical properties – methods. In: Edgar, N.T. & Saunders, J.B. *et al.* (eds) *Initial reports of the Deep Sea Drilling Project*, **15** (e-book).
- Cheng, C.H. & Toksöz, M.N. 1979. Inversion of seismic velocities for the pore aspect ratio spectrum of a rock. *Journal of Geophysical Research*, **84**(B13), 7533–7544.
- Choquette, P.W. & Pray, L.C. 1970. Geological nomenclature and classification of porosity in sedimentary carbonates. *American Association of Petroleum Geologists Bulletin*, **57**(2), 207–250.
- Dunham, R.J. 1962. Classification of carbonate rocks according to depositional texture. In: Ham, W.E. (ed.) *Classification of carbonate rocks: a symposium*. American Association of Petroleum Geologists Memoir, **1**, 108–122.
- Dvorkin, J. & Gutierrez, M.A. 2001. Grain sorting, porosity, and elasticity. Available online at: <http://pangea.stanford.edu/~jack/Bimodal.pdf>.
- Eberli, G.P., Beachle, G.T., Anselmetti, F.S. & Ince, M. 2003. Factors controlling elastic properties in carbonate sediments and rocks. *The Leading Edge*, **22**(7), 654–660.
- Fabricius, I.L. 2002. *Porosity loss in chalk facies sediments by physical compaction or by cementation – Consequences for P-wave modulus*. Paper presented at the American Association of Petroleum Geologists meeting, Houston, Texas.
- Fabricius, I.L. 2003. How burial diagenesis of chalk sediments controls sonic velocity and porosity. *American Association of Petroleum Geologists Bulletin*, **87**(11), 1755–1778.
- Fabricius, I.L. 2007. Chalk: composition, diagenesis and physical properties. *Bulletin of the Geological Society of Denmark*, **55**, 97–128.
- Fabricius, I.L. & Borre, M.K. 2007. Stylolites, porosity, depositional texture, and silicates in chalk facies sediments, Ontong Java Plateau-Grom and Tyra fields, North Sea. *Sedimentology*, **54**, 183–205.
- Fabricius, I.L., Røgen, B. & Gommessen, L. 2007. How depositional texture and diagenesis control petrophysical and elastic properties of samples from five North Sea chalk fields. *Petroleum Geoscience*, **13**, 81–95.
- Grutznher, J. & Mienert, J. 1999. Physical property changes as a monitor of pelagic carbonate diagenesis: An empirically derived diagenetic model for Atlantic ocean basins. *American Association of Petroleum Geologists Bulletin*, **83**(9), 1485–1501.
- Gutierrez, M.A., Dvorkin, J. & Nur, A. 2002. Stratigraphy-guided rock physics. *The Leading Edge*, **21**(1), 98–103.
- Hamilton, E.L., Berger, W.H., Johnson, T.C. & Mayer, L.A. 1982. Acoustic and related properties of calcareous deep-sea sediments. *Journal of Sedimentary Petrology*, **52**(3), 733–753.
- Kim, D.C. & Manghni, M.H. 1992. Influence of diagenesis on the electrical resistivity and the formation factor of deep-sea carbonate sediments. *Geo-Marine Letters*, **12**, 14–18.
- Kroenke, L.W., Berger, W.H. & Janecsek, T.R. *et al.* 1991. *Proceedings of the Ocean Drilling Program, Initial reports*, **130**. Ocean Drilling Program, College Station TX.
- Kuster, G.T. & Toksöz, M.N. 1974. Velocity and attenuation of seismic waves in two-phase media: Part I. Theoretical formulations. *Geophysics*, **39**, 587–606.
- Mavko, G., Mukerji, T. & Dvorkin, J. 1998. *The Rock Physics Handbook*. Cambridge University Press, Cambridge.
- Morse, J.W. & Mackenzie, F.T. 1990. *Geochemistry of sedimentary carbonates*. Developments in Sedimentology, **48**. Elsevier, Amsterdam.
- Nur, A. & Simmons, G. 1969. The effect of saturation on velocity in low porosity rocks. *Earth and Planetary Science Letters*, **7**, 183–193.
- Nur, A., Mavko, G., Dvorkin, J. & Galmudi, D. 1998. Critical porosity: A key to relating physical properties to porosity in rocks. *The Leading Edge*, **17**(3), 357–362.
- Reuss, A. 1929. Berechnung der fließgrenzen von mischkristallen auf grund der plastizitätsbedingung für einkristalle. *Zeitschrift für Angewandte Mathematik und Mechanik*, **9**, 49–58.
- Røgen, B., Gommessen, L. & Fabricius, I.L. 2001. Grain size distribution of chalk from image analysis of electron micrographs. *Computer and Geosciences*, **27**(9), 1071–1080.
- Schlanger, S. & Douglas, R. 1974. The pelagic ooze–chalk–limestone transition and its implications for marine stratigraphy. In: Hsu, K. & Jenkyns, H.C. (eds) *Pelagic Sediments: On Land and Under the Sea*. Special Publication of the International Association of Sedimentologists, **1**, 117–148.
- Schlanger, S., Douglas, R.G., Lancelot, Y., Doherty, L., Moore, T.C. & Roth, P.H. 1973. Fossil preservation and diagenesis of pelagic carbonates from the Magellan Rise, central North Pacific Ocean. In: *The shipboard scientific party, initial reports of the Deep Sea Drilling Project*, **17** (e-book).
- Scholle, P.A. 1977. Chalk diagenesis and its relationship to petroleum exploration: Oil from chalks, a modern miracle? *American Association of Petroleum Geologists Bulletin*, **61**(7), 982–1009.
- Scholle, P.A., Bebout, D.G. & Moore, C.H. 1983. *Carbonate depositional environments*. American Association of Petroleum Geologists Memoir, **33**.
- Schwartz, L.M. & Kimminau, S. 1987. Analysis of electrical conduction in the grain consolidation model. *Geophysics*, **52**(10), 1402–1411.
- Smith, W.H.F. & Sandwell, D.T. 1997. Global seafloor topography from satellite altimetry and ship depth sounding. *Science*, **277**, 1957–1962.
- Sun, Y.F. & Goldberg, D. 1997. Estimation of aspect-ratio changes with pressure from seismic velocities. In: Lovell, M.A. & Harvey, P.K. (eds) *Developments in Petrophysics*. Geological Society, London, Special Publications, **122**, 131–139.
- Wang, Z. 1997. Seismic properties of carbonate rocks. In: Palaz, I. & Marfurt, K.J. (eds) *Carbonate Seismology*. Geophysical Developments, **6**, 29–52.
- Wyllie, M., Gregory, A.R. & Gardner, G.H.F. 1956. Elastic wave velocities in heterogeneous and porous media. *Geophysics*, **21**(1), 41–70.
- Yan, J., Li, X.Y. & Liu, E. 2002. Effects of pore aspect ratios on velocity prediction from well-log data. *Geophysical Prospecting*, **50**, 289–300.

